TRANSONIC ANALYSIS USING A BOUNDARY ELEMENT METHOD

U. Iemma and L. Morino

Terza Università degli Studi di Roma
Rome, Italy

Abstract A boundary element method for the simulation of two- and three-dimensional transonic potential flows is presented. The method is based on a boundary integral equation formulation for the full-potential equation. The latter appears in the form of non-linear wave equation for the velocity potential. All the nonlinear terms, which are expressed in conservative form, are moved to the RHS. This formulation represents a novel approach to the analysis of the full-potential transonic flows using integral methods. Numerical results are obtained for steady two- and three-dimensional transonic flows. The comparison with existing finite-difference and finite-volume results shows a remarkable agreement.

1. Introduction

The present paper deals with a boundary element method (BEM) for the solution of two- and three-dimensional transonic flows, and is based on the work of Iemma.[8] The integral formulation is based on that of Morino,[14] who presents a general theory for potential flows aroud aircraft having arbitrary shape and motion. The main difference of this formulation, with respect to other integral approaches,[21][22][11] is that the full-potential equation appears in the form of nonlinear wave equation. The nonlinear terms are expressed in conservative form, and moved to the RHS of the equation. This yields that the linear differential operator is the D'Alembert operator, whereas, for the other integral approaches is the Laplacian.

In the present work, two different interpretations are presented for the numerical evaluation of the nonlinear terms. In a first formulation (referred in the following as **approach A**), the integral term representing the volume nonlinear sources is integrated by parts (in order to avoid the evaluation of the divergence of $\nabla\phi$), whereas, in the second one (**approach B**), the volume integral is discretized in its original form. Both formulations are applied to subcritical and supercritical, two- and three-dimensional flows. In order to capture shocks, dissipative effects are introduced in the supersonic region of the flow in the form of *artificial compressibility*, linear and nonlinear *artificial viscosity*, and *flux upwinding*.

The formulation of Morino[14] is applied to transonic small perturbation (TSP) by Tseng and Morino,[24] who use approach A and show that the method is able of capturing shocks. Iemma et al.[7] present the first validation of the method for three-dimensional, unsteady, supercritical flows. The first applications of approach A to two-dimensional full-potential analysis is due to Morino and Iemma[16], who present, to the authors' knowledge, the first conservative scheme applied to a boundary integral formulation of the full-potential equation. Approach B was introduced in Iemma.[8] Preliminary applications of approach B to the transonic analysis of helicopter rotors in hover are presented in Iemma, Gennaretti, and Morino.[6]

Section 2 deals with the boundary integral formulation of the full-potential differential model. Even if the formulation is valid for unsteady flows around bodies in arbitrary motion, here we make the assuption that the body moves in uniform translation. The treatment of the nonlinearities is also presented in Section 2. The numerical discretization is briefly outlined in Section 3, whereas, the artificial dissipation schemes are discussed in Section 4. The numerical results presented in Section 5, and compared with finite-element, finite-difference, and finite-volume solutions of both the full-potential and (when applicable) Euler equations.

2. Full-potential integral formulation

The equation governing the motion of an isentropic and irrotational flow, is the full-potential equation,

which is written here in the form of nonlinear wave equation. In a frame of reference rigidly connected with the body (BFR) we obtain

$$\nabla^2\phi - \frac{1}{a_\infty^2}\frac{d_B^2\phi}{dt^2} = \sigma \tag{1}$$

where σ represents all the nonlinear terms, whereas $d_B/dt = \partial/\partial t + U_\infty \partial/\partial x$ is the time derivative written in the BFR (which moves with velocity $\mathbf{v}_B = -U_\infty\,\mathbf{i}$),*i.e.*, following a point fixed in the air frame of reference. Eq. 1 is derived by combining the conservative form of the continuity equation with Bernoulli's theorem for isentropic potential compressible flow, taking into account the isentropic density-hentalpy relation. Indeed, it can be shown that an inviscid non-conducting shock-free flow, initially irrotational and isentropic, remains isentropic and irrotational at all times. The expression for σ is

$$\sigma = \nabla\cdot\mathbf{b} - \frac{d_B\hat{b}}{dt} \tag{2}$$

where

$$\mathbf{b} = \left(1 - \frac{\rho}{\rho_\infty}\right)\nabla\phi \qquad \hat{b} = \frac{\rho}{\rho_\infty} + \frac{1}{a_\infty^2}\frac{d_B\phi}{dt} \tag{3}$$

whereas ρ/ρ_∞ is obtained from the Bernoulli theorem, $\rho/\rho_\infty = \left[1 - \left(\dot{\phi} + v^2/2\right)/h_\infty\right]^{1/\gamma-1}$ (different expressions for the nonlinear terms σ are discussed in Morino and Iemma[16]). In order to isolate the steady part of σ we introduce the notation $\sigma = \nabla\cdot\check{\mathbf{b}} - \partial\hat{b}/\partial t$, where $\check{\mathbf{b}} = \left\{b_x - U_\infty\hat{b}, b_y, b_z\right\}$. The boundary conditions complete the differential problem. These are: the ipermeability of the body surface, $\mathcal{S}_B$, or $\partial\phi/\partial n = \mathbf{v}_B\cdot\mathbf{n}$ for $\mathbf{x}$ on $\mathcal{S}_B$, $\phi = 0$ at infinity. In addition, we have the conditions of no penetration between fluid and wake, and continuity of pressure across the wake surface, $\mathcal{S}_W$. This yield $\Delta(\partial\phi/\partial n) = 0$, $D_W/Dt\,(\Delta\phi) = 0$ for $\mathbf{x}$ on $\mathcal{S}_W$ (where $D_W/Dt = \partial/\partial t + \mathbf{v}_W\cdot\nabla$, and $\mathbf{v}_W$ is the velocity of a point of the wake); $D_W/Dt\,(\Delta\phi) = 0$ states that $\Delta\phi$ is constant in time following a wake point $\mathbf{x}_W$ and equal to the value it had when $\mathbf{x}_W$ left the trailing edge. In addition, we introduce homogeneous initial conditions.

The integral formulation for the differential problem presented is outlined in the following. Since we deal, in the present paper, with applications to fixed wing analysis, the integral equation presented is limitated to bodies in uniform translation. As mentioned above, the extension of the analysis to flows around bodies in arbitrary rigid motion (helicopter rotors and propeller) is presented in Iemma, Gennaretti, Morino[6] and in Iemma[8].

The fundamental solution G for Eq. 1 is the solution of the problem

$$\nabla^2 G - \frac{1}{a_\infty^2}\frac{d_B^2\phi}{dt^2}G = \delta(\mathbf{x}-\mathbf{x}_*)\delta(t-t_*) \tag{4}$$

where δ denotes the Dirac delta function. The initial and infinity boundary conditions associated with the above problem are, respectively, $\dot{G}(\mathbf{x},\infty) = G(\mathbf{x},\infty) = 0$, and $G(\infty,t) = 0$. The expression of G for subsonic flows is[14]

$$G(\mathbf{x},\mathbf{x}_*,t,t_*) = \frac{-1}{4\pi r_\beta}\delta(t-t_*+\theta) \tag{5}$$

where $r_\beta(\mathbf{x},\mathbf{x}_*) = \sqrt{M_\infty^2(x-x_*)^2 + \beta^2 r^2}$ and $\theta(\mathbf{x},\mathbf{x}_*) = (1/a_\infty\beta^2)\left[r_\beta + M_\infty(x-x_*)\right]$ with $M_\infty = U_\infty/a_\infty$, $\beta = \sqrt{1-M_\infty^2}$ and $r = \|\mathbf{r}\| = \|\mathbf{x}-\mathbf{x}_*\|$.

The integral formulation of the problem is obtained by multiplying Eq. 1 by G and Eq. 4 by ϕ, subtracting, and integrating in time and over the entire domain $\mathcal{V}$. Applying the Gauss theorem, using the boundary condition at infinity for G and ϕ, and integrating with respect to time (taking into account the initial conditions on ϕ and G), introducing the Prandtl-Glauert variables, $x_0 = x/\beta$, $y_0 = y$, $z_0 = z$, yields

$$\begin{aligned}\phi(\mathbf{x}_*,t_*) = &\oint\!\!\!\!\!\!\int_{\mathcal{S}_{B_0}}\left[G_0\frac{\partial\phi}{\partial n_0} - \phi\frac{\partial G_0}{\partial n_0} + \frac{\partial\phi}{\partial t}G_0\frac{\partial\hat{\theta}_0}{\partial n_0}\right]^{\theta_0} d\mathcal{S}_0 \\ &- \iint_{\mathcal{S}_{W_0}}\left[\Delta\phi\frac{\partial G_0}{\partial n_0} - \frac{\partial\Delta\phi}{\partial t}G_0\frac{\partial\hat{\theta}_0}{\partial n_0}\right]^{\theta_0} d\mathcal{S}_0 \\ &+ \iiint_{\mathcal{V}_0} G_0\,[\sigma]^{\theta_0}\,d\mathcal{V}_0\end{aligned} \tag{6}$$

where, $G_0 = -1/4\pi r_0$, with $r_0 = \|\mathbf{x}_0 - \mathbf{x}_{0_*}\|$, whereas $[...]^{\theta_0}$ denotes evaluation at the retarded time $t = t_* - \theta_0$, with $\hat{\theta}_0 = [r_0 - M_\infty(x_0 - x_{0_*})]/a_\infty\beta$. Moreover, $\mathcal{S}_{B_0}$ and $\mathcal{S}_{W_0}$ are the surfaces of the body and of the wake in the Prandtl-Glauert space, whereas $\partial/\partial n_0$ denotes the normal derivative.

If $\sigma = 0$ (*i.e.*, in the linear case) and $\mathbf{x}_* \in \mathcal{V}$, Eq. 6 is an integral representation of $\phi(\mathbf{x}_*,t_*)$ as a function of ϕ, $\partial\phi/\partial n_0$ on $\mathcal{S}_{B_0}$ and of $\Delta\phi$ on $\mathcal{S}_{W_0}$. On the other hand, if $\mathbf{x}_*$ is on $\mathcal{S}_B$, Eq. 6 represents a compatibility condition between ϕ and $\partial\phi/\partial n_0$ on $\mathcal{S}_{B_0}$ and $\Delta\phi$ on $\mathcal{S}_{W_0}$ for any function ϕ satisfying Eq. 1. Since $\partial\phi/\partial n$ is known from the boundary conditions, and $\Delta\phi$ from the preceding time history, then Eq. 6 yields a boundary integral equation for ϕ. In the nonlinear case ($\sigma \neq 0$) we take advantage of the evaluation of nonlinear terms at retarded times. Indeed, only the current value of σ needs to be extracted (by numerical differentiation) from ϕ in the field, whereas the retarded one is known from previous time steps.

Two different approaches are introduced in order to evaluate numerically the volume integral of equation 6. In the first one (referred as **approach A**), an

integration by parts of the nonlinear integral term is introduced, in order to avoid the evaluation of the divergence operator. Specifically, considering that $\left[\nabla \cdot \check{\mathbf{b}}\right]^{\theta} = \nabla \cdot \left[\check{\mathbf{b}}\right]^{\theta} + \left[\partial \check{\mathbf{b}}/\partial t\right]^{\theta} \cdot \nabla\theta$ (subscript 0 has been dropped in order to simplify the notations), and applying the divergence theorem, we obtain

$$\iiint_{\mathcal{V}} G\,[\sigma]^{\theta}\,d\mathcal{V} = -\oint\!\!\!\oint_{\mathcal{S}_B} \left[\mathbf{n}\cdot\check{\mathbf{b}}\right]^{\theta} G\,d\mathcal{S} \qquad (7)$$
$$-\iiint_{\mathcal{V}} \left[\check{\mathbf{b}}\right]^{\theta}\cdot\nabla G\,d\mathcal{V} + \iiint_{\mathcal{V}} \left[\frac{\partial \hat{b}}{\partial t} + \frac{\partial \check{\mathbf{b}}}{\partial t}\cdot\nabla\theta\right]^{\theta} G\,d\mathcal{V}$$

This approach, with the assumption of small perturbation, has been applied in the past to the analysis of two- and three-dimensional unsteady transonic flows around fixed and rotary wings,[24][7][15] and extended by the authors to the full-potential analysis.[16][8]

In the second approach (**approach B**) the volume integral is discretized in its original form. Approach B appears to be computationally convenient with respect to approach A, as we will see in the next section.

3. Numerical discretization

In order to solve numerically the problem, the above integral equation is discretized using a zeroth-order formulation. The surface of the body is divided into M elements $\mathcal{S}_m$, that of the wake into N elements $\mathcal{S}_n$ and the fluid volume into Q volume elements $\mathcal{V}_q$. Using the collocation method, and setting the collocation points at the centers of elements, approach A yields

$$\begin{aligned}\phi_k(t) &= \sum_{m=1}^{M} B_{km}\,[\bar{\chi}_m]^{\theta_{0_{km}}} + \sum_{m=1}^{M} C_{km}\,[\phi_m]^{\theta_{0_{km}}} \\ &+ \sum_{m=1}^{M} D_{km}\,[\dot{\phi}_m]^{\theta_{0_{km}}} + \sum_{n=1}^{N} F_{kn}\,[\Delta\phi_n]^{\theta_{0_{kn}}} \\ &+ \sum_{n=1}^{N} G_{kn}\,[\Delta\dot{\phi}_n]^{\theta_{0_{kn}}} + \sum_{q=1}^{Q} \mathbf{H}_{kq}\cdot[\check{\mathbf{b}}_{0_q}]^{\theta_{0_{kq}}} \\ &+ \sum_{q=1}^{Q} \bar{\mathbf{H}}_{kq}\cdot[\dot{\check{\mathbf{b}}}_{0_q}]^{\theta_{0_{kq}}} + \sum_{q=1}^{Q} \hat{H}_{kq}[\dot{\hat{b}}_q]^{\theta_{0_{kq}}} \qquad (8)\end{aligned}$$

(where $\bar{\chi}_m = \partial\phi/\partial n_0 - \mathbf{n}_0(\mathbf{x}_m)\cdot\check{\mathbf{b}}_0(\mathbf{x}_m)$, and $[...]^{\theta_{0_{km}}}$ denotes evaluation at the retarded time $t - \theta_{0_{km}}$), whereas for approach B one obtains

$$\begin{aligned}\phi_k(t) &= \sum_{m=1}^{M} B_{km}\,[\chi_m]^{\theta_{0_{km}}} + \sum_{m=1}^{M} C_{km}\,[\phi_m]^{\theta_{0_{km}}} \\ &+ \sum_{m=1}^{M} D_{km}\,[\dot{\phi}_m]^{\theta_{0_{km}}} + \sum_{n=1}^{N} F_{kn}\,[\Delta\phi_n]^{\theta_{0_{kn}}} \\ &+ \sum_{n=1}^{N} G_{kn}\,[\Delta\dot{\phi}_n]^{\theta_{0_{kn}}} + \sum_{q=1}^{Q} H_{kq}[\sigma_{0_q}]^{\theta_{0_{kq}}} \qquad (9)\end{aligned}$$

The coefficients of the linear part of equations 8 and 9 are identical for both the formulation

$$B_{km} = \iint_{\mathcal{S}_m} G_{0_k} d\mathcal{S},\; C_{km} = \iint_{\mathcal{S}_m} \frac{\partial G_{0_k}}{\partial n_0} d\mathcal{S},\; ... \qquad (10)$$

whereas the nonlinear ones are considerably different. Indeed, for approach A we have

$$\begin{aligned}\mathbf{H}_{kq} &= -\iiint_{\mathcal{V}_q} \nabla_0 G_{0_k} d\mathcal{V} \\ \bar{\mathbf{H}}_{kq} &= \iiint_{\mathcal{V}_q} G_{0_k}\,\nabla_0\theta_k d\mathcal{V} \qquad (11) \\ \hat{H}_{kq} &= \iiint_{\mathcal{V}_q} G_{0_k} d\mathcal{V}\end{aligned}$$

whereas for approach B we have

$$H_{kq} = \iiint_{\mathcal{V}_q} G_{0_k} d\mathcal{V} \qquad (12)$$

In addition, we have

$$[\sigma]^{\theta} \approx \overline{\nabla\cdot\left[\check{\mathbf{b}}\right]^{\theta}} + \left[\frac{\partial \hat{b}}{\partial t} + \frac{\partial \check{\mathbf{b}}}{\partial t}\cdot\nabla\theta\right]^{\theta} \qquad (13)$$

where $\overline{\nabla\cdot\left[\check{\mathbf{b}}\right]^{\theta}}$, the mean value of $\nabla\cdot\check{\mathbf{b}}$ on each element, is calculated as the flux of $\check{\mathbf{b}}$ through the boundary $\partial\mathcal{V}_q$

$$\begin{aligned}\overline{\nabla\cdot\left[\check{\mathbf{b}}\right]^{\theta}}\Big|_q &= \frac{1}{\mathcal{V}_q}\iiint_{\mathcal{V}_q} \nabla\cdot\left[\check{\mathbf{b}}\right]^{\theta} d\mathcal{V} \\ &= \frac{1}{\mathcal{V}_q}\oint\!\!\!\oint_{\partial\mathcal{V}_q} \left[\check{\mathbf{b}}\right]^{\theta}\cdot\mathbf{n}\,d\mathcal{S} \qquad (14)\end{aligned}$$

being $\mathbf{n}_q$ the unit normal to the surface $\partial\mathcal{V}_q$. Note that the first formulation requires the evaluation of seven coefficients for each pair kq (two vector quantities plus a scalar one), whereas only one single scalar is needed in the second approach. Considering that the number of nonlinear coefficients is proportional to the square of the number of elements in the field, can be easily seen that approach B is much more convenient from a numerical point of view, in both terms of computer time and storage space.

4. Artificial dissipation

In order to capture shocks, the present formulation needs the addition of dissipative effects in the supersonic region of the flows. The first form of conservative artificial dissipation for a boundary integral formulation is presented in Morino and Iemma [16]. The

schemes presented here are the extensions of that first approach to different forms of the dissipative terms. In particular, four different schemes are considered and applied to the boundary integral equation presented above. In approach A, the artificial dissipation is included in the form of linear and nonlinear *artificial viscosity*, as well as *artificial compressibility*, whereas, for approach B, a *flux upwinding* technique is applied in the evaluation of $\check{\mathbf{b}} \cdot \mathbf{n}$ on $\partial \mathcal{V}_q$. All these concept are an adaptation to the boundary integral equation method of existing CFD techniques (see Ref.[16] and[8] for a historical review).

Artificial viscosity

In approach A, a technique for including dissipative effects in the full-potential equation deals with the addition of artificial viscous terms within the supersonic region of flow. These terms should be proportional to upwind derivatives of the velocity in the local direction of the flow. This technique could be considered as a direct evolution of the original *type-dependent differencing*, introduced by Murman and Cole[18] for the non conservative TSP equation, extended to conservative TSP by Murman[17], and to the full-potential equation by Jameson for both the non conservative[9] and the conservative[10] forms of the equation. The adaptation to the present boundary integral equation formulation is considered in two different ways. In the first one, the viscous correction is introduced at the level of the evaluation of the $x-$component of the velocity. The modified quantity has the form

$$\tilde{u} = \phi_x^c - \Delta s \frac{\partial}{\partial s}\left(\mu \frac{\partial \phi}{\partial s}\right) \tag{15}$$

where ϕ_x^c indicates the centered finite difference approximation for the $x-$derivative of the potential, and $\mu(M)$ represents the switching function that activates the dissipation terms where $M > 1$. The typical expression suggested in the literature for μ is $\mu(M) = C \max\left[0, 1 - M_c/M^2\right]$, where M_c is a *cut-off* Mach number, and C is a constant. The use of M_c was introduced in order to avoid the occurrence of instabilities, due to the discontinuity of the slope of the function $\mu(M) \in C^0$. This is accomplished by moving the commutation slightly below the sonic point. A new expression for the switching function is introduced by Iemma[8] in order to achieve the same stability with $M_c = 1$. The function $\mu(M) \in C^\infty$ is

$$\mu(M) = \frac{C}{1 + e^{-\lambda(M+M_0)}} \tag{16}$$

where λ controls the slope of the function at $M = M_0$. Numerical experiments revealed an increased stability using the Eq. 16. This formulation has been applied to two- and three-dimensional analysis, revealing a good agreement with other numerical solution of full-potential and Euler equation.

The expression of $\tilde{u}$ in Eq. 15 is introduced in the Bernoulli theorem (to evaluate ρ/ρ_∞), and then in Eq.2. It can be shown that the dissipative term actually added to the inviscid nonlinear term is nonlinear. In the second approach, the artificial viscosity term is introduced as an artificial mass-flux in the evaluation of the nonlinear source terms

$$\tilde{\sigma} = \sigma + \Delta s \frac{\partial}{\partial x}\left[\mu \frac{\partial}{\partial s}\left(\frac{\partial \phi}{\partial x}\right)\right] \tag{17}$$

After the integration by parts (approach A) the above expression assumes the form

$$\tilde{\mathbf{b}}_k = \check{\mathbf{b}}_k - \Delta s \, \mu_k \left.\frac{\partial u}{\partial s}\right|_k \mathbf{i} \tag{18}$$

where $\mathbf{i}$ represents the unit vector of the x direction. The latter approach yields a linear artificial viscous term. This peculiarity seems to have a favorable influence on the stability of the iteration process.

Artificial compressibility

Still for approach A, including the dissipative effects only in the calculation of the density, results in a different interpretation of the artificial dissipation terms. This point of view, first proposed by Eberle[2], generalized by Hafez, South and Murman[4] and Holst and Ballhaus,[5] and known as *artificial compressibility*, has been successfully applied in the past to the finite element solution of the full potential equation. The adaptation to the boundary integral formulation is very simple. Consider the modified density

$$\tilde{\rho} = \rho - \mu(M)\, \Delta s \frac{\partial \rho}{\partial s} \tag{19}$$

where s is the streamwise direction, the dissipative effects are introduced by substituting ρ with $\tilde{\rho}$ in the calculation of the nonlinear terms

$$\tilde{\mathbf{b}} = \left(1 - \frac{\tilde{\rho}}{\rho_\infty}\right) \nabla \phi - U_\infty \left(\frac{\tilde{\rho}}{\rho_\infty} + \frac{U_\infty}{a_\infty^2} \frac{\partial \phi}{\partial x}\right) \tag{20}$$

Flux upwinding

In approach B the nonlinear terms are not integrated by parts, and the evaluation of $\nabla \cdot \check{\mathbf{b}}$ is reduced to the evaluation of the flux of $\check{\mathbf{b}}$ through the boundary of each element $\mathcal{V}_q$. The introduction of dissipative terms in such a formulation can be easily done using a so-called *flux upwinding* scheme. This class of dissipation schemes derive from an accurate reformulation of the artificial dissipation concepts, in

order to develop monotone converging schemes for the numerical solution of the Euler equation. First application of this technique are due to Engquist and Osher[3] for the small-disturbance equation, and to Osher[19] for the full-potential equation. A very general form for these schemes can be given by denoting with $f_{i-1/2,j}$, $f_{i+1/2,j}$, $f_{i,j+1/2}$, $f_{i,j-1/2}$ the mass flux flowing through the four faces of the element surrounding the control point $\mathbf{x}_{ij}$, and by identifying i as the index following the local stream direction. Dissipative effects are introduced at supersonic points by means of the modified flux $f^d_{i\pm1/2,j}$

$$f^d_{i\pm1/2,j} = f_{i\pm1/2,j} - D_{i\pm1/2,j} \tag{21}$$

where D represents a general form of dissipation. In the present formulation we have $f_{i\pm1/2,j} = \check{\mathbf{b}} \cdot \mathbf{n}|_{i\pm1/2,j}$, and for the additive term D a first order expression is used. We obtain

$$f^d_{i\pm1/2,j} = f_{i\pm1/2,j} - \mu_{i\pm1/2,j} \left.\frac{\partial f}{\partial s}\right|_{i\pm1/2,j} \Delta s \tag{22}$$

This scheme, limited here to two dimensions for sake of clarity, has been successfully applied to three-dimensional problems. Higher-order dissipation schemes, involving second derivatives of the density, are currently under investigation.

5. Numerical results

The formulation presented above has been applied to the analysis of steady two- and three-dimensional transonic flows around fixed wings. Particular emphasis is given to the validation of the algorithm in subcritical and supercritical regimes, through comparison with existing numerical solutions of the full-potential and Euler equation. Indeed, as mentioned above, the full-potential model is exactly equivalent to the complete Euler model, since no entropy or vorticity sources (such as strong shock waves) are present in the field. Moreover, even if weak shock waves occur, comparisons between the two formulations are meaningful, since the entropy jump introduced by the shock remains negligible. The applications presented in the following deal with both approach A (nonlinear terms integrated by parts) and approach B (nonlinear terms in divergence form). Two-dimensional, steady, subcritical (no shock waves) problems are presented first, and compared to numerical solution of the Euler equation, in order to validate the nonlinear algorithm. Note that the steady solution is obtained by marching in time, and that a two-dimensional problem is approximated by a three-dimensional one with very high aspect ratio. Results of a convergence analysis are also presented. Two-dimensional steady supercritical problem are then analyzed. Comparisons with existing numerical solutions of the full potential and Euler equation are presented, including the validation of the dissipation schemes described above. Finally, preliminary results obtained for three-dimensional steady transonic flows about fixed wings are presented.

Two-dimensional subcritical

In order to assess the accuracy of the nonlinear potential model, the present method has been applied to two-dimensional subcritical cases, and compared to numerical solution of the Euler equation. Two different tests are considered: the flow around a circular cylinder at $M_\infty = 0.38$, and a NACA 0012 airfoil flying at $M_\infty = 0.63$ with angle of attack $\alpha = 2^o$. These test cases are choosen just below the critical (*i.e.*, sonic) conditions, in order to ensure a strong influence of the nonlinear terms, and, at the same time, to guarantee the isentropicity of the flow. The results of the present methodology are compared to accurate numerical solution of the Euler equations obtained by Lerat[13] and Dadone[1]. Figure 1 depicts the velocity potential distribution on the surface of the cylinder at $M_\infty = 0.38$. The nonlinear solution is compared to the linear potential, in order to verify the influence of the nonlinearities. The solution is strongly affected by the nonlinear terms, as confirmed by the pressure coefficient distribution, presented in Fig. 2. The prediction of the nonlinear boundary integral nonlinear formulation shows a remarkable agreement with both Euler solutions. The convergence of the nonlinear terms appears to be very fast, as shown in Fig. 3, where the time history of the quantity $|RHS_{n+1} - RHS_n| / |RHS_1|$ is presented (RHS represents all the nonlinear terms of Eqq. 8 and 9. As we will see, the convergence rate depends on the regularity of the computational mesh. Non uniform meshes require a higher number of iteration to reach convergence. Indeed, a non uniform grid is used for the test case of Figs. 4, 5, 6 (NACA 0012 airfoil at $M_\infty = 0.63$ and angle of attack $\alpha = 2^o$). The solution is still very accurate in terms of pressure distribution when compared to the Euler solutions,[13][1] but the steady state is reached after a higher number of steps. Nevertheless, this number remains considerably lower than that required by other CFD methods.

Convergence analysis The subcritical problems presented have been used as test cases in order to evaluate the rate of convergence of the numerical solution as the number of elements increases. Results obtained by the convergence analysis are presented in Figs. 7, 8 (for approach A) and 9 (for approach B). The control parameter used for the non lifting flow around the

cylinder is the local value of pressure coefficients on the body at $\theta = \pi/2$, whereas, for the lifting flow, is the lift coefficient C_L. The boundary integral solution converges to a value very close to that predicted by Lerat.[13] This is not surprising, since the numerical solution obtained by Dadone[1] is affected, as stated by the author, by a numerical production of vorticity, inconsistent with the potential flow assumption. When we focus our attention to an integral quantity, such as the lift coefficient, these small differences totally disappear. The boundary integral solution converges to a value in excellent agreement with both the Euler solutions, and this is true for approach A (Fig. 8), as well for approach B (Fig. 9).

Two-dimensional supercritical

The present boundary integral method is capable of capturing sharp shocks, when they occur. Fig. 10 depicts the pressure distribution on the surface of a cylinder at $M_\infty = 0.5$. The integral solution (approach A with nonlinear artificial viscosity) for two different mesh sizes is compared to finite volume full-potential solution.[20] In this particular case, no Euler solutions are considered as reference results, since the strenght of the shock yields a strong entropy jump; in this condition, potential and Euler model are no longer comparable. The discontinuity in pressure predicted by the integral method appears as an actual jump, confined within one single element. The agreement with the finite volume result is very good in terms of shock position and intensity. Note that the convergence of the solution to the steady state is extremely fast and monotone (see Fig. 11). This occurs, in our experiences, whenever a regular O-type grid is used,

Fig. 12 deals with a non-lifting NACA 0012 airfoil flying at $M_\infty = 0.82$. The velocity potential distribution obtained with both boundary integral approaches is presented. The shock appears as a sharp discontinuity for the potential slope, smeared only by the numerical discretization used to evaluate the pressure from the potential. In Fig. 13 the pressure distribution is compared to finite volume solution of both full-potential and Euler equations. This is meaningful, since the entropy jump introduced by the shock is negligible (weak shock). Note that the pressure coefficient distribution obtained by approach B reveals, after the sonic point, some differences with respect to the reference results. This lack of accuracy, confined within the supersonic region of the domain, is attributed to the different impact of the artificial dissipation schemes used in the two formulation.[8] The H-type mesh used in the computation is stretched and not uniformly distributed. The convergence rate to the steady state (Fig. 14) is higher than in the preceding case in agreement with what stated above.

In the results presented above, the dissipative effects are introduced in approach A in the form of *nonlinear artificial viscosity*, whereas, in approach B, using the *flux-upwinding* technique. Two additional schemes have been applied to approach A, in order to verify the applicability to a boudary integral formulation of concepts inspired by other CFD methods. In particular, dissipation is included as *artificial compressibility*, or in the form of *linear artificial viscosity*. The results are presented in Fig. 15. The test case deals with a biconvex parabolic airfoil, with thickness ratio 0.2, at $M_\infty = 0.82$. Since the concept of modified density has been widely investigated in the past within the framework of the finite element method, a finite element solution for the full-potential equation is used as reference result.[12] The pressure coefficient distribution presents a shock discontinuity, which appears sharper for the integral solution. The agreement is good for both the formulation, even if the artificial compressibility approach presents a shock intensity slightly increased. Furthermore, the latter approach, which is nonlinear, presents a slower convergence of the iteration to the stady state, as shown in Fig. 16. Note that in both cases $\mu(M) \in C^\infty$.

Three-dimensional supercritical

In this section, preliminary three-dimensional results are presented. Fig. 17 depicts the pressure coefficient distribution on the upper and lower surfaces of a rectangular biconvex-section wing with aspect ratio 4, thickness 6%, and angle of attack $\alpha = 1.5^o$, at $M_\infty = 0.857$. The integral solution is obtained using approach B. The comparison with a finite difference solution[23] for the root section (Fig. 18) reveals a good agreement in terms of position and intensity of the shock. Validation of the approach A has not yet been performed for this particular test case (because the higher computational effort required overtakes the storage capacity of the available machine). In order to compare the two boundary integral approaches, a non-lifting flow around a swept, tapered wing has been examined with both the formulations. In this case we take advantage of the z-symmetry of the flow, in order to save CPU time and storage capacity. The wing section is a NACA 0012 airfoil, the sweep angle is $\Lambda = 10^o$, and the Mach number at infinity is $M_\infty = 0.82$. Figs. 19 and 20 depict the pressure distribution on the wing surface, whereas Fig. 21 presents the comparison of the two formulations for the root section. The latter reveals that, in the three-dimensional analysis, approach A predicts a shock slightly weaker than that obtained using approach B. The reasons for this behaviour (totally absent in the two-dimensional analysis) is currently

under investigation.

References

[1] A. Dadone. Computation of transonic steady flows using a modified lambda formulation. In A. Dervieux, B. Van Leer, J. Periaux, and A. Rizzi, editors, *Numerical Simulation of Compressible Euler Flows*, GAMM Workshop, pages 122–137, Braunschweig, 1986. Vieweg & Sohn.

[2] A. Eberle. A finite element method for the solution of transonic potential flows around airfoils. Technical Memorandum 75324, NASA, June 1977.

[3] B. Engquist and S. Osher. Stable and entropy satisfying approximation for transonic potential flow calculation. *Mathematics of Computation*, 34(149):45–75, January 1980.

[4] Mohammed M. Hafez, M. M. South, and E. M. Murman. Artificial compressibility method for the numerical solution of the full potential equation. *AIAA Journal*, 17(6):838–844, 1978.

[5] T.L. Holst and W.F. Ballhaus. Fast, conservative schemes for the full potential equation applied to transonic flows. *AIAA Journal*, 17(4):145–52, 1979.

[6] U. Iemma, M. Gennaretti, and L. Morino. Boundary element method for unified transonic aerodynamic and aeroacoustic analyses of rotors. In 19^{th} *European Rotorcraft Forum Proc.*, Cernobbio, Italy, 1993.

[7] U. Iemma, F. Mastroddi, L. Morino, and M. Pecora. A boundary integral formulation for unsteady transonic potential flow. In *AGARD Specialists' Meeting on Transonic Unsteady Aerodynamics and Aeroelasticity*, number 507, San Diego, California, 1991.

[8] Umberto Iemma. *Metodi integrali in aerodinamica transonica.* Tesi di dottorato di ricerca in ingegneria aerospaziale, Università degli Studi di Roma *La Sapienza*, Roma, 1994.

[9] Antony Jameson. Iterative solutions of transonic flows over airfoils and wings, including flows at mach 1. *Comm. Pure and Applied Mathematics*, 27:283–309, 1974.

[10] Antony Jameson. Transonic potential flow calculation using conservation form. In *AIAA Second Computational Fluid Dynamics Proceedings*, pages 148–161, Hartford Connecticut, 1975.

[11] Osama A. Kandil and Hong Hu. Full-potential integral solution for transonic flows with and without embedded euler domains. *AIAA Journal*, 26(9), 1988.

[12] D. J. Kinney. *Finite Element Simulation of Compressible Inviscid and Viscous Flows.* tesi di PhD, University of California, 1989.

[13] A. Lerat and J. Sides. Implicit transonic calculations without artificial viscosity or upwinding. In A. Dervieux, B. Van Leer, J. Periaux, and A. Rizzi, editors, *Numerical Simulation of Compressible Euler Flows*, GAMM Workshop, pages 227–250, Braunschweig, 1986. Vieweg & Sohn.

[14] L. Morino. A general theory for unsteady compressible potential aerodynamics. Contractor Report CR-2464, NASA, 1974.

[15] L. Morino, M. Gennaretti, U. Iemma, and F. Mastroddi. Boundary integral transonics for wings and rotors. *Aerotecnica Missili e Spazio*, 71(1-2):52–61, January-June 1992.

[16] L. Morino and U. Iemma. Boundary integral equations and conservative dissipation schemes for full-potential transonic flow. *Computational Mechanics*, 13(1/2):90–100, 1993.

[17] Earll M. Murman. Analisys of embedded shock waves calculated by relaxation methods. *AIAA Journal*, 12(5):626, May 1974.

[18] Earll M. Murman and Julian D. Cole. Calculation of plane steady transonic flows. *AIAA Journal*, 9(1):114, January 1971.

[19] S. Osher. Shock modelling in aeronautics. In K.W. Morton and M.J. Baines, editors, *Numerical Methods for Fluid Dynamics*, pages 1179–218. Academic Press, London, 1982.

[20] M. D. Salas. Recent developments in transonic euler flow over a circular cylinder. Technical Memorandum 83282, NASA, Langley Research Center, Hampton, Virginia, april 1982.

[21] P. M. Sinclair. An exact integral (field panel) method for the calculation of 2-dimensional transonic potential flow around complex configuration. *Aeronautical Journal*, 90:227, June-July 1986.

[22] P. M. Sinclair. A three-dimensional field integral method for the calculation of transonic flow on complex configuration - theory and preliminary results. *Aeronautical Journal*, page 235, June-July 1988.

[23] J. L. Steger and F. X. Caradonna. A conservative finite difference algorithm for the unsteady transonic full potential equation. Technical Memorandum 81211, NASA, October 1980.

[24] Kadin Tseng and Luigi Morino. Nonlinear green's function method for unsteady transonic flows. In David Nixon, editor, *Transonic Aerodynamics*, number 81 in Progres in Astronautics ans Aeronautics. 1982.

Figures

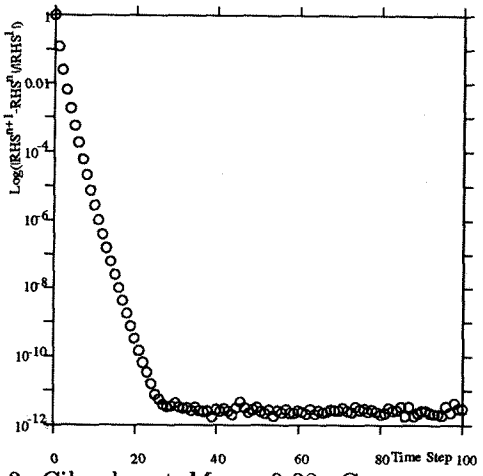

Figure 3: Cilynder at $M_\infty = 0.38$. Convergence history. Approach A.

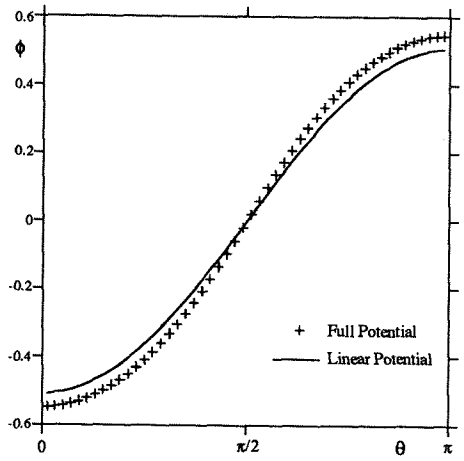

Figure 1: Cilynder at $M_\infty = 0.38$. Velocity potential: linear and nonlinear solutions. Approach A.

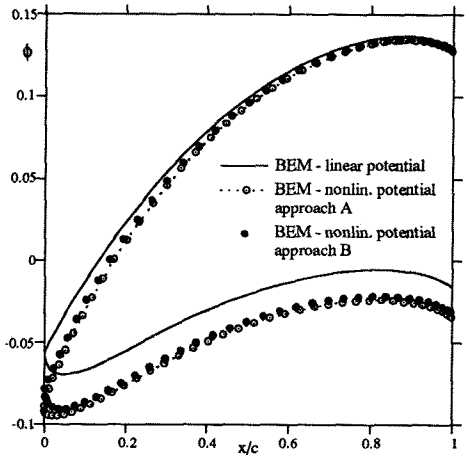

Figure 4: NACA 0012, $M_\infty = 0.63$, $\alpha = 2^o$. Vel. potential: linear and nonlinear solutions.

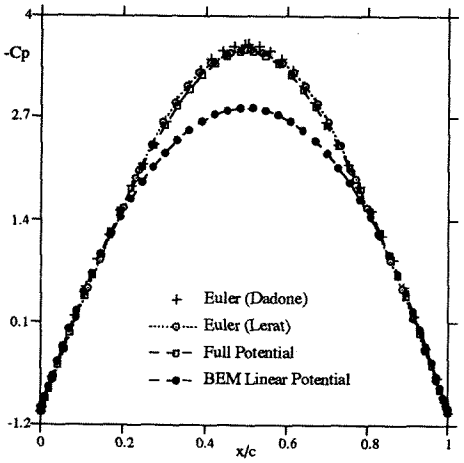

Figure 2: Cilynder at $M_\infty = 0.38$. Pressure coeff.: linear and nonlinear potential vs. Euler solutions. Approach A.

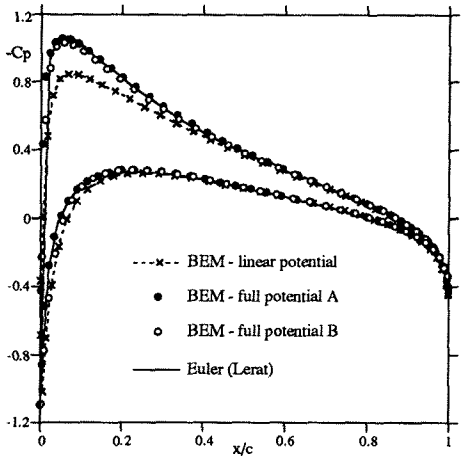

Figure 5: NACA 0012, $M_\infty = 0.63$, $\alpha = 2^o$. Pressure coeff.: linear and nonlin. potential vs. Euler.

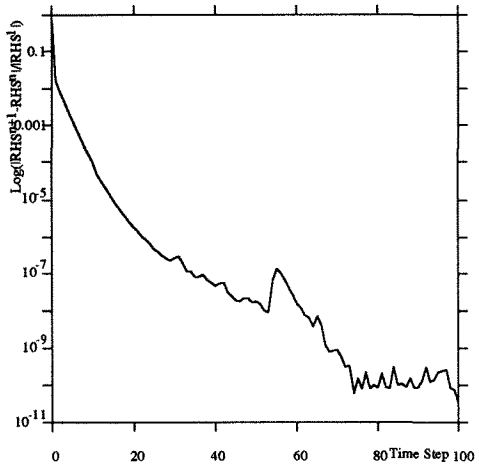

Figure 6: NACA 0012, $M_\infty = 0.63$, $\alpha = 2^o$. Convergence history. Approach A.

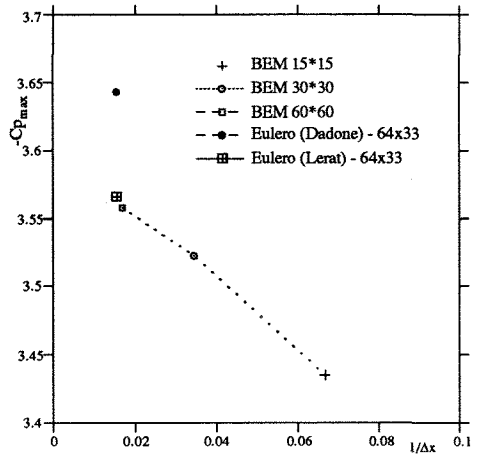

Figure 7: Cilynder at $M_\infty = 0.38$. Convergence for $\Delta x \to 0$. Approach A.

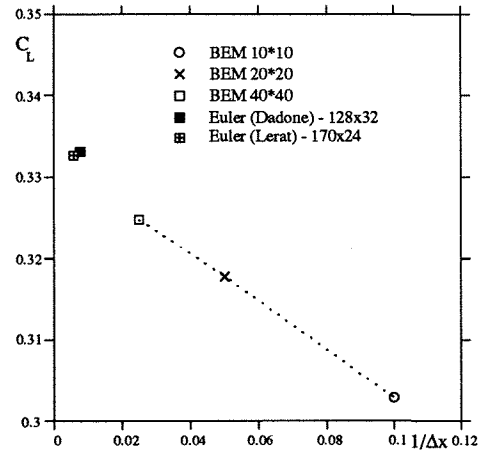

Figure 8: NACA 0012, $M_\infty = 0.63$, $\alpha = 2^o$. Convergence for $\Delta x \to 0$. Approach A.

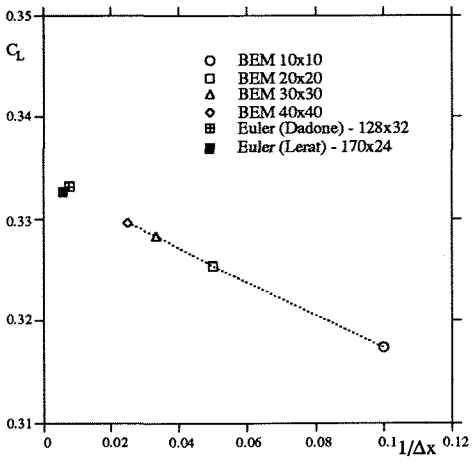

Figure 9: NACA 0012, $M_\infty = 0.63$, $\alpha = 2^o$. Convergence for $\Delta x \to 0$. Approach B.

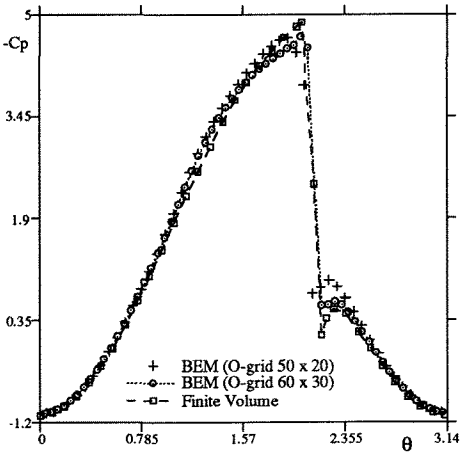

Figure 10: Cilynder at $M_\infty = 0.5$. Pressure coefficient. Approach A.

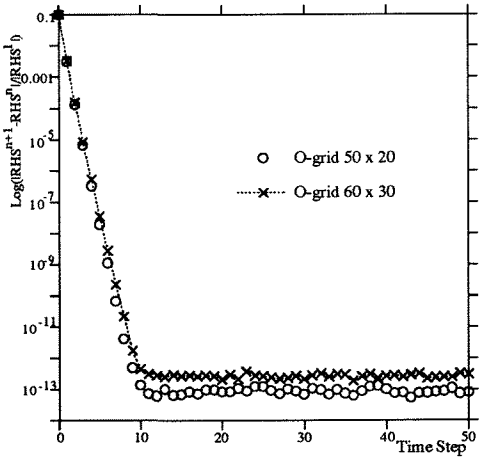

Figure 11: Cilynder at $M_\infty = 0.5$. Convergence history. Approach A.

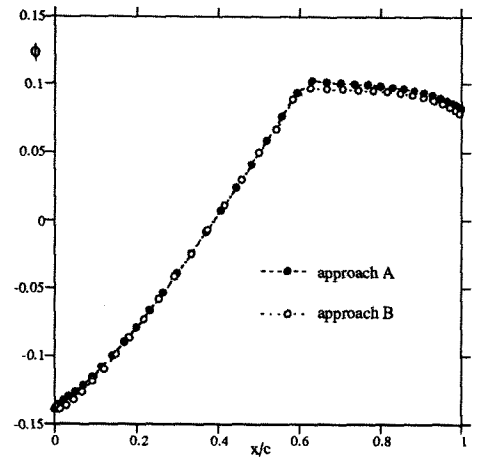

Figure 12: NACA 0012, $M_\infty = 0.82$, $\alpha = 0^o$. Velocity potential.

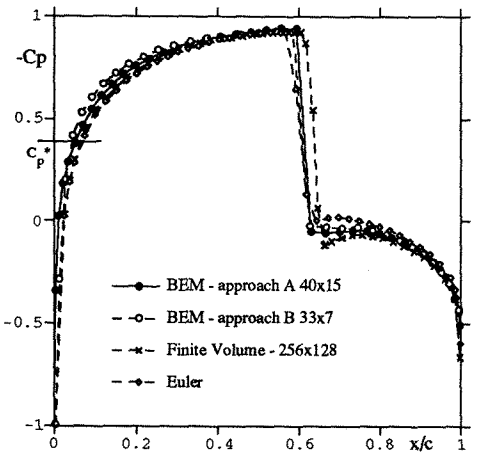

Figure 13: NACA 0012, $M_\infty = 0.82$, $\alpha = 0^o$. Pressure coefficient.

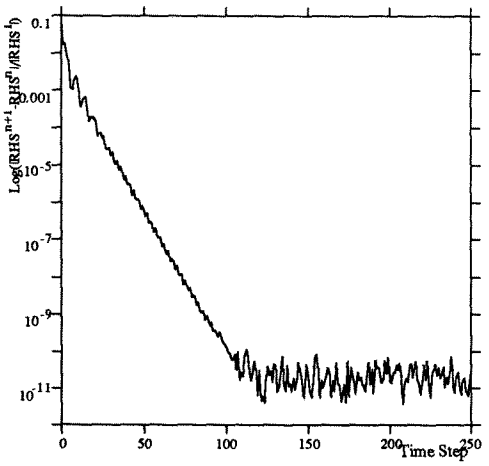

Figure 14: NACA 0012, $M_\infty = 0.82$, $\alpha = 0^o$. Convergence history. Approach A.

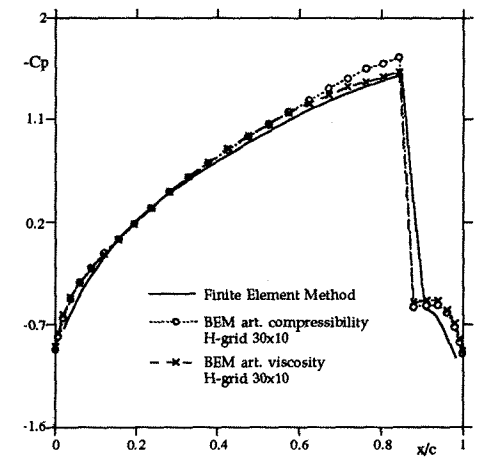

Figure 15: 20% parabolic arc, $M_\infty = 0.82$, $\alpha = 0^o$. Art. dissipation schemes. Approach A.

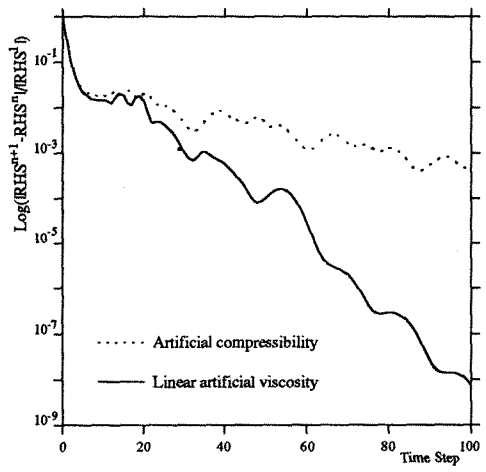

Figure 16: 20% parabolic arc, $M_\infty = 0.82$, $\alpha = 0^o$. Convergence history. Approach A.

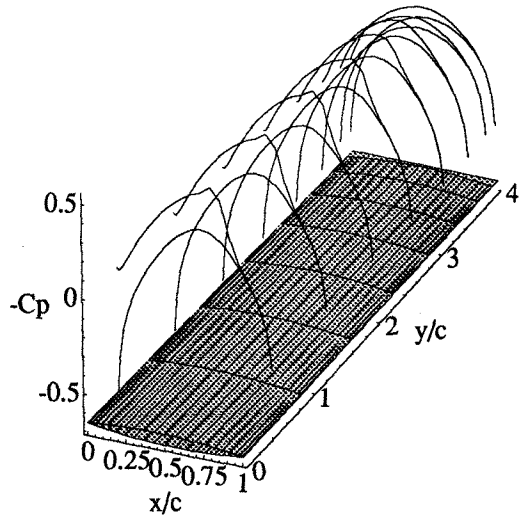

Figure 17: Rectangular wing, $AR = 4$, biconvex 6%, $M_\infty = 0.857$, $\alpha = 1.5^o$. Pressure coefficient. Approach B.

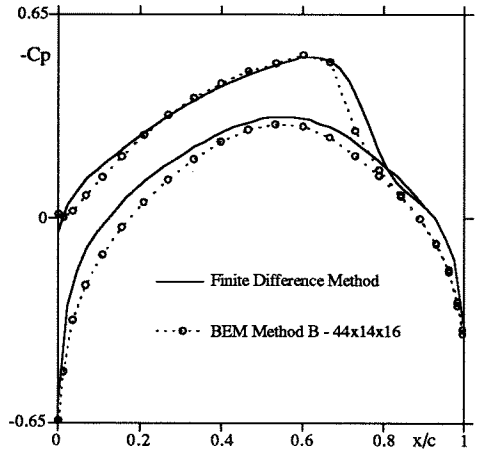

Figure 18: Rectangular wing, $AR = 4$, biconvex 6%, $M_\infty = 0.857$, $\alpha = 1.5^o$. Pressure coefficient at the root section.

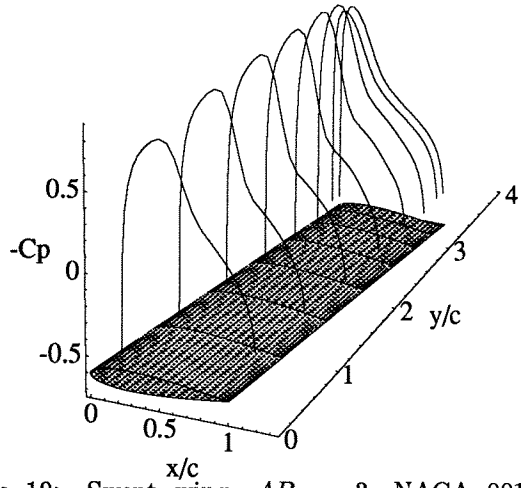

Figure 19: Swept wing, $AR = 3$, NACA 0012, $M_\infty = 0.82$, $\alpha = 0^o$, sweep angle $\Lambda = 10^o$. Pressure coefficient. Approach A.

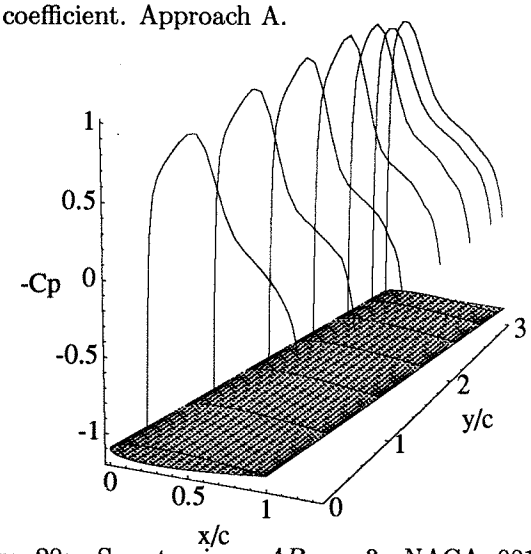

Figure 20: Swept wing, $AR = 3$, NACA 0012, $M_\infty = 0.82$, $\alpha = 0^o$, sweep angle $\Lambda = 10^o$. Pressure coefficient. Approach B.

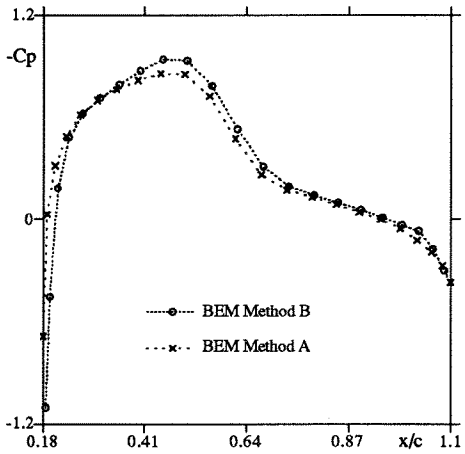

Figure 21: Swept wing, $AR = 3$, NACA 0012, $M_\infty = 0.82$, $\alpha = 0^o$, sweep angle $\Lambda = 10^o$. Pressure coefficient at $y/c = 1.044$ section.